Vibrational Spectroscopy and X-ray Diffraction of Cd(OH)$_2$ to 28 GPa at 300 K

Sang-Heon Shim* and Sandeep Rekhi

Department of Earth, Atmospheric, and Planetary Sciences,

Massachusetts Institute of Technology, Cambridge, MA 02139

Michael C. Martin

Advanced Light Source Division, Lawrence Berkeley National Lab, Berkeley, CA 94720

Raymond Jeanloz

Department of Earth and Planetary Science,

University of California, Berkeley, CA 94720

(Dated: March 16, 2006)

Abstract

We report Raman and infrared absorption spectroscopy along with X-ray diffraction for brucite-type β-Cd(OH)$_2$ to 28 GPa at 300 K. The OH-stretching modes soften with pressure and disappear at 21 GPa with their widths increasing rapidly above 5 GPa, consistent with a gradual disordering of the H sublattice at 5–20 GPa similar to that previously observed for Co(OH)$_2$. Asymmetry in the peak shapes of the OH-stretching modes suggests the existence of diverse disordered sites for H atoms in Cd(OH)$_2$ under pressure. Above 15 GPa, the A_{1g}(T) lattice mode shows non-linear behavior and softens to 21 GPa, at which pressure significant changes are observed: new Raman modes appear, two Raman-active lattice modes and the OH-stretching modes of the low-pressure phase disappears, and the positions of some X-ray diffraction lines change abruptly with the appearance of weak new diffraction features. These observations suggest that amorphization of the H sublattice is accompanied by a crystalline-to-crystalline transition at 21 GPa in Cd(OH)$_2$, which has not been previously observed in the brucite-type hydroxides. The Raman spectra of the high-pressure phase of Cd(OH)$_2$ is similar to those of the high-pressure phase of single-crystal Ca(OH)$_2$ of which structure has been tentatively assigned to the Sr(OH)$_2$ type.

I. INTRODUCTION

High symmetry prompts considering the brucite-type hydroxides [M(OH)$_2$, M = Mg, Ca, Ni, Co, Fe, Mn, Cd] as a model for understanding the bonding of hydrogen within crystal structures. In geophysics, high-pressure studies of this structure have provided valuable information about the role of hydrogen in hydrous and nominally anhydrous minerals[1].

The brucite structure is characterized by a hexagonal unit cell with cation–oxygen layers stacked along the c-axis. A hydrogen atom is attached to each oxygen atom. At ambient pressure, an O–H bond is aligned along the c-axis and points toward an empty tetrahedron surrounded by three cation–oxygen octahedra in the neighboring layer (Fig. 1a). Each H atom is surrounded by three H atoms attached to the neighboring layer (H$\cdots$H in Fig. 1). With pressure, the structure initially compresses mostly along the c-axis and the interlayer spacing decreases while the cation-oxygen layers remain relatively uncompressed[2–5]. This promotes the interaction among H and O atoms in the neighboring layers (O$\cdots$H and H$\cdots$H in Fig. 1), as is suggested by the decrease in frequency and broadening of the OH-stretching vibration observed for all brucite-type hydroxides studied to date with compression[6–9].

In addition, brucite-type hydroxides exhibit diverse behavior at high pressure. A reversible amorphization of the entire crystal structure has been reported for Ca(OH)$_2$ compressed to 11 GPa at room temperature[6,10–12]. However, single-crystal Ca(OH)$_2$ undergoes a transition to a crystalline phase, likely Sr(OH)$_2$-type, at 6 GPa followed by reversible amorphization around 20 GPa at room temperature[13]. In Co(OH)$_2$, the hydrogen (H) sublattice becomes amorphized at 11 GPa, while the Co–O sublattice remains in a crystalline state[14,15]. In contrast, Mg(OH)$_2$ remains stable and does not amorphize to at least 34 GPa (Ref. 6).

The nature of the strong interaction among H and O atoms in the neighboring layers of the brucite-type structures at high pressure remains controversial. Earlier experiments[6] proposed that the negative shift and broadening of the OH-stretching vibration is due to a strengthening of hydrogen bonding between H and O atoms in adjacent layers (O$\cdots$H in Fig. 1). A later neutron diffraction study[3] reported lengthening of the O–D bonds with pressure, consistent with a strengthening of hydrogen bonding at high pressure. However, a molecular dynamics simulation[16] suggests that amorphization of the H sublattice results from frustration of H atoms by the interplay of short-range repulsion and electrostatic forces.

β-Cd(OH)$_2$ is an interesting case because many of its structural parameters, such as c/a, O—O, O$\cdots$H, and $\angle$O$\cdots$O—H (Table I), are similar to those of Ca(OH)$_2$ at ambient conditions. In particular, β-Cd(OH)$_2$ is more compact along the c-axis (i.e., has the smallest c/a ratio and interlayer spacing) than any other brucite-type hydroxides at ambient pressure. Yet the O$\cdots$H distance in Cd(OH)$_2$ remains one of the longest among the hydroxides. This is mainly due to the fact that the O–H units are distant from each other along the a-axis, in comparison with the other hydroxides (see O—O in Table I). Among the transition-metal hydroxides (M = Ni, Co, Fe, Mn, and Cd), the magnitudes of the bond lengths and angle are the largest for Cd(OH)$_2$ (Table I). Therefore, it is of particular interest to compare the behavior of Cd(OH)$_2$ to Ca(OH)$_2$ and other transition-mental hydroxides under pressure. In addition, compounds with larger cations tend to show a given sequence of structural changes at lower pressures than those with smaller cations, and Cd is the largest among the brucite-type hydroxides listed in Table I. We have therefore investigated the high-pressure behavior of Cd(OH)$_2$ using Raman and infrared absorption spectroscopy along with X-ray diffraction.

II.   EXPERIMENTAL TECHNIQUES

Synthetic β-Cd(OH)$_2$ (Aldrich Chemicals, purity 99.99%) was loaded in a 150 μm hole of a 20–30 μm thick indented stainless steel gasket sandwiched between two diamond anvils of a symmetric diamond-anvil cell. All experiments were conducted at room temperature and pressure was measured using the ruby fluorescence scale[17].

For Raman measurements we used a pair of diamond anvils with ultra-low fluorescence. These were performed at MIT using a dispersive-Raman system consisting of an Ar/Kr mixed-ion laser, a single spectrometer, and a liquid nitrogen cooled CCD up to 28 GPa (Fig. 2a-c). We focused a 514.5-nm laser beam on the sample to excite the Raman modes and the sampling time was typically 5 minutes. The emission spectrum of neon was used to calibrate the spectrometer. We conducted measurements with Ar as a pressure medium (quasi-hydrostatic, QH) and without any pressure medium (non-hydrostatic, NH) in order to determine the effects of deviatoric stresses at high pressure, and did not resolve any systematic differences between these different runs.

Some IR-active lattice modes have been observed in previous Raman measurements on

$Mg(OH)_2$ (Ref. 18) and $Co(OH)_2$ (Ref. 15). Similarly, we observe a mode at 270 cm^{-1} from the sample, with a pressure-induced shift of 5.2 cm^{-1}/GPa, when we use a laser power exceeding 3 mW. The frequency at ambient conditions shows reasonable agreement with an IR-active $E_u(T)$ mode (264 cm^{-1}, Ref. 19) and we avoid this spectral contamination by regulating the laser power below 0.5 mW throughout our measurements.

Synchrotron-based infrared (IR) absorption spectroscopy was performed up to 25 GPa using beam line 1.4.3 at the Advanced Light Source, with samples loaded in an Ar pressure medium (Fig. 2d). In comparison with bench-top FTIR, the advantages of synchrotron-based FTIR include a 2–3 order-of-magnitude enhancement in flux and reduction of the beam to a 10 μm diffraction-limited diameter[20]. Background spectra were measured for areas filled only with Ar in the sample chamber and were subtracted from raw IR spectra of the samples. The IR measurements were conducted in an open atmosphere. Although much of the water signal has been nulled in the data processing, some absorption remains and this becomes noticeable in spectra measured at high-pressure, where the signal from the sample becomes very weak (Fig. 2d). In analysis of the spectroscopy data, symmetric peaks were fitted to pseudo-Voigt profile shape functions. We used a split pseudo-Voigt function for asymmetric peaks.

Angle-dispersive powder X-ray diffraction measurements were performed up to 36 GPa at the GSECARS beam line of the Advanced Photon Source, the 10.3 sector of the Stanford Synchrotron Radiation Laboratory, and the B-2 beamline of the Cornell High Energy Synchrotron Source using imaging plates with beam energy of 24 keV (20 μm in diameter), 17 keV (50 μm in diameter), and 25 keV (35 μm in diameter), respectively. Cubic boron nitride, which is semi-transparent to the X-ray beam, was used as seats for the diamonds in order to increase the diffraction angle to 24°2θ. The sample-to-detector distances were measured using the diffraction from CeO_2, NaCl, and MgO. To determine pressure, we used either ruby[17] or gold[21] in different X-ray diffraction runs, and the samples were loaded either in a CsCl pressure medium or without a pressure medium. Two-dimensional diffraction images were integrated to one-dimensional diffraction patterns using the FIT2D program[22] and individual peaks were fitted using a pseudo-Voigt profile function. Unit-cell parameters and volume were calculated using the UNITCELL program[23].

III. RESULTS

A. Vibrational spectroscopy

For the brucite-type hydroxides, the lattice modes are translational $[A_{1g}(\text{T})$, $A_{2u}(\text{T})$, $E_g(\text{T})$, and $E_u(\text{T})]$ and librational $[E_g(\text{R})$ and $E_u(\text{R})]$, and internal modes originate from symmetric [Raman active, $A_{1g}(\text{OH})$] and antisymmetric [IR active, $A_{2u}(\text{OH})$] OH-stretching vibrations. We observed Raman modes at 235 cm^{-1} $[E_g(\text{T})]$, 384 cm^{-1} $[A_{1g}(\text{T})]$, and 3566 cm^{-1} $[A_{1g}(\text{OH})]$ at ambient conditions (Figs 2, 3, and 6), consistent with earlier reports[19] (238, 384, and 3566 cm^{-1}). The librational mode of β-Cd(OH)$_2$ and other transition-metal hydroxides have not been documented in the literature, but we observed a mode at 755 cm^{-1} at ambient conditions in samples recovered from high pressure. This mode is also observed at high pressure (Figs 2 and 6), and its low intensity and large width are consistent with expectations for the libration mode, $E_g(\text{R})$. The librational modes are observed at 680 and 725 cm^{-1} in Ca(OH)$_2$ and Mg(OH)$_2$, respectively, so we tentatively assign the 755 cm^{-1} mode to the librational mode of β-Cd(OH)$_2$. In IR measurements, we observed the $A_{2u}(\text{OH})$ mode at 3605 cm^{-1} at 1.8 GPa which agrees with previous measurements[19] at ambient conditions (3607 cm^{-1}) after accounting for the pressure-induced shift in frequency.

Both Raman- and IR-active OH-stretching modes decrease in frequency and intensity with pressure (Figs 2c and d). The frequency of the $A_{1g}(\text{OH})$ mode decreases linearly $(-4.1\pm0.4$ cm^{-1}/GPa) on compression to 10 GPa, becomes less sensitive to pressure between 10 and 20 GPa $(-0.8\pm0.2$ cm^{-1}/GPa), and drops by 23 cm^{-1} before disappearing at 21 GPa (Fig. 3). Above 21 GPa, we do not detect any mode other than a very weak feature at 3580 cm^{-1} in an internal-mode range (ν_7 in the inset of Fig. 2c).

Upon decompression, the $A_{1g}(\text{OH})$ mode re-appears at 20 GPa with some degree of hysteresis in the frequency to 10 GPa (Fig. 3). Below 10 GPa, the frequencies agree well with each other on compression and decompression. The weak feature (ν_7) observed above 21 GPa becomes noticeably intense on decompression and persists to 7 GPa (Fig. 2c). Its weak intensity and severe overlap with the strong $A_{1g}(\text{OH})$ mode makes it difficult to precisely track its frequency, but this mode appears to be much less sensitive to pressure in comparison with $A_{1g}(\text{OH})$ (Fig. 3).

Our IR data exhibit interference patterns in the background, likely caused by the di-

amond anvils, and these affect peak fitting (Fig. 2d). However, we can still resolve the behavior of the $A_{2u}(OH)$ mode under pressure, with a frequency decreasing linearly to 10 GPa (-1.4 ± 0.8 cm^{-1}/GPa) and becoming almost insensitive to pressure between 10 and 20 GPa (-0.1 ± 0.4 cm^{-1}/GPa), in qualitative agreement with our observations for the $A_{1g}(OH)$ mode (Fig. 3). The $A_{2u}(OH)$ mode also weakens and broadens with pressure, and finally becomes barely resolved above 19 GPa (Fig. 2d), and on decompression it re-appears at 19 GPa with some degree of hysteresis.

The frequency of ν_7 observed in Raman spectra appears to coincide with that of the IR-active $A_{2u}(OH)$ mode between 10 and 20 GPa. Previous high-pressure studies on brucite-type hydroxides have likewise documented IR-active modes in Raman spectra[15,24] and vice-versa[14]. However, ν_7 is still observed above 21 GPa even though the $A_{2u}(OH)$ mode has disappeared (Fig. 3). Furthermore, the fullwidth at half maximum (FWHM) of ν_7 is much smaller than that of the $A_{2u}(OH)$ mode (Fig. 2), so it is unlikely that ν_7 is the IR-active OH-stretching mode. Above the amorphization pressure of $Ca(OH)_2$, a weak mode is also observed (at 3638 cm^{-1}) with a slightly negative pressure shift[10]. This mode is remarkably similar to ν_7 of $Cd(OH)_2$.

Negative pressure shifts are well-documented for the $A_{1g}(OH)$ and $A_{2u}(OH)$ frequencies of other brucite-type hydroxides, and are generally assumed to arise from increased hydrogen bonding[6] or enhanced electrostatic interactions[16] among H and O atoms in the neighboring layers decreasing the force constant of the O–H bond. Compared to the other brucite-type hydroxides, the rate of frequency decrease of $A_{1g}(OH)$ is the lowest for $Cd(OH)_2$, perhaps due to the fact that $Cd(OH)_2$ has the smallest c/a ratio and interlayer spacing yet the largest O—O distance (Table I). The steep initial decrease in the c/a ratio does not change interactions among the O–H units as effectively as in the other hydroxides, because in $Cd(OH)_2$ the O–H units are much more distant from each other along the a- than the c-axis in comparison with any other brucite-type hydroxides. Both OH-stretching modes show saturation of the negative mode shifts near 10 GPa (Fig. 3), consistent with our findings by X-ray diffraction that $Cd(OH)_2$ becomes very incompressible above 10 GPa (see below). Thus, changes in the bond lengths and angles would be smaller above 10 GPa, making the interactions among neighboring-layer H and O atoms less sensitive to pressure.

The $A_{1g}(OH)$ mode of $Cd(OH)_2$ exhibits broadening with pressure with an increase of the rate of change at 5 GPa (Fig. 4) and no significant hysteresis observed on decompression.

The broadening is also observed for the $A_{2u}(OH)$ mode, again with an increase rate of change above 5 GPa although less-well resolved due to the difficulties mentioned above (Fig. 4).

Pressure-induced broadening of the OH-stretching modes in the brucite-type hydroxides has been attributed to disordering of the O–H bonds[6,8,9,14] (Fig. 4). A Raman study of $Ca(OH)_2$ reported a steep increase in FWHM above 11 GPa (Ref. 10), whereas $Mg(OH)_2$ shows a monotonous increase up to 34 GPa (Ref. 18). An increase in broadening rates of the OH-stretching modes was observed above 10 GPa in $Co(OH)_2$ (Refs 7,14,15). The magnitudes and behavior of the FWHM of the OH-stretching modes of $Cd(OH)_2$ are comparable to those observed for $Ca(OH)_2$ and $Co(OH)_2$ with the broadening rate of $A_{1g}(OH)$ for $Cd(OH)_2$ is between those for $Co(OH)_2$ and $Ca(OH)_2$. Near 20 GPa, the magnitude of the FWHM of the OH-stretching modes in $Cd(OH)_2$ becomes similar to those of $Ca(OH)_2$ and $Co(OH)_2$ near the region of the pressure at which the H sublattice is inferred to amorphize. Thus, we conclude that the H sublattice of $Cd(OH)_2$ also disorders gradually between 5 and 20 GPa.

The shapes of the OH-stretching peaks become increasingly asymmetric with pressure to 5 GPa (Figs 2c, 2d, and 5), whereas the lattice modes are well fitted with a symmetric profile. The asymmetry parameter shown in Fig. 5 increases steeply up to 5 GPa and becomes less sensitive to pressure above 10 GPa. We found no systematic difference in this parameter between runs with and without an Ar pressure medium, implying that the asymmetry is not caused by deviatoric stress. Our IR spectra do not provide sufficient resolution to measure the asymmetry parameter precisely, but it is notable that this is the first report of significant asymmetry in the OH-stretching modes in a brucite-type hydroxide at high pressure.

Asymmetric peak shapes have been observed for the OH-stretching modes of some materials. The Raman-active mode of water bearing SiO_2 glass shows strong anisotropy, with the lower-frequency side side being broader than the higher-frequency side[25], similar to our observation for $Cd(OH)_2$. The asymmetry was attributed to the existence of a range of hydrogen-bonding environment[25]: the higher-frequency side of the peak would represent O–H groups associated with weaker or no hydrogen bonding whereas the lower-frequency side of the peak would indicate the presence of diverse range of stronger hydrogen-bonded environment. An asymmetric OH-stretching mode was also reported in hydrous wadsleyite[26] for which a high degree of disordering among several different sites was documented by ^{1}H MAS NMR (Ref. 27).

The translational lattice modes stiffen linearly to 15 GPa (Figs 2a and 6). Above 15 GPa, the E_g(T) mode becomes very weak (Fig. 2a) and the pressure-induced shift of the A_{1g}(T) mode becomes non-linear and finally shows softening as 20 GPa is approached (Fig. 6). Above 10 GPa, we also observe a noticeable intensity increase for the lower-frequency shoulder of the A_{1g}(T) mode ($\sim$430 cm^{-1}). Inclusion of a new peak at this position significantly improves our spectrum fitting above 15 GPa (ν_3 in Fig. 2a). The position of this peak shows scatter in Fig. 6 because of its small intensity and severe overlap with strong adjacent peaks. Nevertheless, we find that this peak persists up to the highest pressure we reached. The appearance of this peak coincides with the pressure where $Cd(OH)_2$ becomes incompressible as documented by X-ray diffraction (see below), but we do not observe any changes in diffraction patterns below 21 GPa. If this is a new phonon mode, the combined vibrational spectroscopy and X-ray diffraction results suggest that $Cd(OH)_2$ undergoes a minor modification or distortion in crystal structure. It is notable that the intensity of this peak is more pronounced in non-hydrostatic runs (i.e., without pressure medium).

At 21 GPa, significant changes are observed in the lattice modes: both lattice modes of β-$Ca(OH)_2$ disappear and new modes appear at 260 (ν_1), 360 (ν_2), and 477 (ν_4) cm^{-1} (see the spectra at 20.5 and 27.9 GPa in Fig. 2). Except for ν_1, which is very difficult to resolve under non-hydrostatic conditions, data from runs with and without and Ar pressure medium agree with each other. We infer that ν_2 and ν_4 are from a crystalline phase because their FWHM are smaller than those of A_{1g}(T) and E_g(T). The three new modes shift linearly with pressure and persist to 28 GPa, the peak pressure of our Raman measurements. These changes in the lattice modes indicate that the Cd–O sublattice undergoes a structural transition.

Upon decompression, some degree of hysteresis is observed for the mode frequencies of ν_1, ν_2, ν_3, and ν_4 with larger $d\nu/dP$ on decompression (Fig. 6). However, the apparent slope changes in ν_1 and ν_3 could be due to the difficulty in reliably fitting the positions of the weak peaks. In comparison, ν_2 is well-resolved and the mode shift of ν_4 is reversible during decompression (Fig. 2a). These new modes persist below 21 GPa and disappear at 10 GPa except for ν_2. In fact, ν_2 shifts toward E_g(T) with decompression and follows the trend of E_g(T) below 5 GPa. The A_{1g}(T) mode re-appears at 22 GPa during decompression and gains intensity with a decrease of pressure (Fig. 2a), showing a reversible frequency shift during decompression. The spectra obtained from recovered samples agree well with those obtained before compression (Fig. 2a), indicating that the high-pressure phase is not

quenchable. However, the observation of the new modes during decompression to 10 GPa indicates that the high-pressure phase does persist metastably over a significant pressure range at room temperature.

The librational mode, $E_g(\text{R})$, is difficult to observe at ambient conditions, but we observe the mode at 779 cm^{-1} at 2.5 GPa. This peak gains intensity with pressure and becomes clear above 8 GPa (Fig. 2b), exhibiting a non-linear mode shift with pressure: $d\nu/dP$ is higher below 10 GPa and above 20 GPa than between 10 and 20 GPa (Fig. 6). The mode again becomes very weak above 21 GPa (Fig. 2b), and it reverts without hysteresis upon decompression, remaining as a weak feature at 755 cm^{-1} in the recovered sample. For comparison, the $E_g(\text{R})$ mode was not detected in $Mg(OH)_2$ or $Ni(OH)_2$ under pressure (Refs 8,18), but it has been detected with a linear increase with pressure up to 31 GPa in $Co(OH)_2$ (Ref. 15).

Lutz et al.[19] took the librational mode frequency as a proxy for the interaction among adjacent O–H units, with a higher frequency indicating stronger interaction. The steeper increase of the librational mode of $Cd(OH)_2$ below 10 GPa is mainly due to the fact that the distance between O–H units decreases due to preferential compression along the c-axis, although the magnitude of the distance decrease should not be as large as observed in the other brucite-type hydroxides based on the mode shift of the OH-stretching vibration. The diminished slope between 10 and 20 GPa is due to stiffening of the structure as observed by X-ray diffraction (see below). After the phase transition at 21 GPa, the librational mode becomes more sensitive to pressure again.

A new mode appears on the higher-frequency side of the librational mode above 5 GPa (ν_6 in Figs 2b and 6). At 21 GPa, another new mode appears on the lower-frequency side of the librational mode (ν_5 in Figs 2b and 6). Both modes show linear increases in frequency with pressure, indicating that these are not from the diamond anvils. In fact, we observe a peak from the diamond anvil at 1110 cm^{-1} and it shows little pressure-induced shift. Thus, ν_6 could be related to a modification or distortion of the Cd–O sublattice as there is no evidence from X-ray diffraction of any phase transition around 5 GPa. The appearance of the ν_5 mode at 21 GPa coincides with significant changes in the other lattice modes, as well as changes in the diffraction patterns (see below), so we identify this mode with a phase transition emerging at 21 GPa.

B. X-ray Diffraction

X-ray diffraction measurements to 37 GPa (Fig. 7) help us interpret the spectroscopic measurements. We observed the diffraction lines of β-Cd(OH)$_2$ up to 21 GPa with no new peaks appearing below 21 GPa (Figs 7a-c). Above 21 GPa, diffraction lines become weak and broad, (010) line shape becomes asymmetric, and some weak features appear near (011) (Fig. 7e) (note that in order to avoid overlapping diffraction lines, gold was not loaded in the runs of Fig. 7e-g). The (001) line also disappears at this pressure, but its intensity is already weakening at lower pressures and this is likely due to the development of preferred orientation of crystals with pressure. The remaining lines and the new features persist to 37 GPa, suggesting that Cd(OH)$_2$ retains some long-range ordering of the Cd–O sublattice at least up to the peak pressure reached in our experiments.

The new features disappear on decompression below 20 GPa (Fig. 7f), but all the other diffraction lines remain broad to 5 GPa. That the (001) line does not re-appear until 5 GPa on decompression supports the idea that the its disappearance above 21 GPa is at least partly due to strong texturing. All the major diffraction lines of the low-pressure phase are then recovered upon complete unloading (Fig. 7f), and these results are in good agreement with our Raman observations for the lattice modes: a crystalline-to-crystalline transition takes place at 21 GPa and the high-pressure phase survives upon decompression to 10 GPa.

We observe that the c-axis is a factor of 3.7 times more compressible than the a-axis. The c/a ratio of Cd(OH)$_2$ decreases steeply below 5 GPa and more gently above 10 GPa (Fig. 8). Because of the evidence for a phase transition at 21 GPa, the Miller indices of the lower-pressure phase are no longer valid above 21 GPa. Nevertheless, we calculate hexagonal unit-cell parameters from the positions of the (010) and (011) lines in order to document the effect of pressure on the structure at pressure above 21 GPa (note that the c/a ratios are determined by at least 6–7 different lines at pressure below 21 GPa). The c/a value then shows a discrete change at 21 GPa, supporting our inference that Cd(OH)$_2$ transforms to a crystalline phase. According to our Raman measurements, both the high- and low-pressure phases coexist during decompression to 10 GPa. Thus, the observed c/a ratio during decompression may be contaminated by diffraction peak overlaps between the low- and high-pressure phases. Nevertheless, little hysteresis is observed in the c/a ratio during decompression. This may indicate that the high-pressure phase may be spectroscopically

more active than the low-pressure phase and/or the amount of the high-pressure phase below 20 GPa is smaller than that of the low-pressure phase.

The c/a ratio of the other brucite-type hydroxides exhibit a similar behavior[11,14,28,29] (Fig. 8). The initial rapid decrease in the c/a ratio has been attributed to the presence of weak O–H bonds in the c-direction and the relatively rigid cation–oxygen octahedra forming layers parallel to the a-axis. Thus, most of the strain on compression is expected to be accommodated along the c-direction as compare to the cation-oxygen plane[2]. However, once the c/a ratio reaches a certain value, it stops changing, perhaps due to an increase of the repulsive force between adjacent H atoms brought into proximity by the compression along the c-axis.

The volume of $Cd(OH)_2$ is plotted as a function of pressure in Fig. 9, where we show a fit of the data between 0 and 21 GPa to the 3rd order Birch-Murnaghan equation of state. The fit yields a pressure derivative of the bulk modulus (at zero pressure), $K_0' = 10.6$, the highest value among the brucite-type hydroxides which typically lie near 5 (Table II). Our X-ray measurements were conducted with a solid medium or with no pressure medium, so it is possible deviatoric stresses play a role for such a high value. Nevertheless, considering the fact that the values of K_0' differ by less than 20–25 % between non- and quasi-hydrostatic measurements for $Mg(OH)_2$, the K_0' of $Cd(OH)_2$ has to be considered abnormally high (Table II). The abnormally high K_0' value may be related to $Cd(OH)_2$ having the smallest c/a ratio and interlayer spacing of the brucite-type hydroxides (Table I). Because $Cd(OH)_2$ has the smallest interlayer spacing at ambient conditions, a small contraction along the c-axis can induce significant repulsion between atoms in the neighboring layers. Thus, the axial compressibility along the c-axis will become small and may be even comparable to that along the a-axis which is controlled by the more rigid CdO_6 octahedra, as shown in the c/a ratio. We tentatively calculate the volume above 21 GPa using the unit cell of the brucite-type structure and find a volume drop of 5% at 21 GPa.

IV. DISCUSSION

The changes observed in $Cd(OH)_2$ below 20 GPa are similar to those in $Co(OH)_2$, which exhibit rapid broadening of the OH-stretching modes and the c/a ratio becoming insensitive to pressure above 11 GPa (Refs 14,15). Above 20 GPa, the rate of the negative shift of the

$A_{1g}(OH)$ mode becomes gradually smaller and the widths of the OH-stretching modes do not change with pressure[15]. Therefore, as in $Co(OH)_2$ (Refs 14,15), we infer that the rapid broadening of the OH-stretching modes between 5 and 20 GPa indicates gradual disordering of the H sublattice in $Cd(OH)_2$. At 20 GPa before the OH-stretching modes disappear, their FWHM reach 150–250 cm^{-1}. As pointed out in previous studies[14,15], this magnitude is comparable to those observed in hydrogen-bearing oxide glasses, water, and some dense-hydrous minerals with disordered H sublattice, indicating amorphization of the H sublattice in $Cd(OH)_2$ at this pressure.

The OH-stretching modes of $Cd(OH)_2$, however, show a significant degree of asymmetry in their peak shape, whereas no evidence of asymmetry was reported for $Co(OH)_2$ (Ref. 15). As pointed out above, the asymmetry may indicate the existence of a range of distinct environment for the H atoms in $Cd(OH)_2$.

One way of explaining the range of H environments in $Cd(OH)_2$ is that these are related to the unusually large distance between the O–H units along the a-axis as compared with the other brucite-type hydroxides, such as $Co(OH)_2$. Neutron diffraction studies[4,30,31] have suggested that the H position in some brucite-type materials can be described by a three-site disordered model (Fig. 1b): H atoms are displaced from the threefold axis, $2d$ sites $(1/3, 2/3, z)$, to three symmetry-related positions around the threefold axis with an equal probability of occupancy, $6i$ sites $(x, 2x, z)$. Parise et al.[32] considered two different cases for the three-site disordered model for $Co(OD)_2$ (Fig. 1b). Assuming that the minimum distance between non-bonded H atoms (H$\cdots$H) is 1.8 Å in ionic systems, they found that neither XGT ($x > 1/3$ for $6i$ sites) nor XLT ($x < 1/3$ for $6i$ sites) sites alone can form an extended structure with D$\cdots$D larger than 1.8 Å. Instead, a mixture of XLT and XGT sites is needed and this allows for only one particular set of site mixing below 10 GPa for $Co(OD)_2$. Above 10 GPa, the mixing site model no longer provides any arrangements with acceptable D$\cdots$D distances[32]. Thus, they proposed that the D(or H) atoms exist in a range of positions along circles with a constant distance from the threefold axis over the pressure range that the OH-stretching mode broadens rapidly.

Assuming that the magnitude of the H displacement in $Cd(OH)_2$ is the same as that in $Co(OH)_2$ at ambient conditions, we examine whether XLT or XGT can yield an extended structure in $Cd(OH)_2$. The 10% larger O–O distance in $Cd(OH)_2$ makes the distance between different H sites greater than 1.8 Å for all but the 1–1′ case (1.3 Å) (e.g., 1–2′ or 1–3′ =

2.00 Å; 2–3′ or 3–2′ = 2.30 Å; 2–2′ or 3–3′ = 2.33 Å in Fig. 1b) in the case of the XGT model. All H$\cdots$H distances are larger than 1.8 Å for the XLT model (e.g., a–c' or b–c' = 2.21 Å; c'–c = 2.52 Å; a–b' or b–a' = 1.88 Å; a–a' or b–b' = 1.92 Å in Fig. 1b). This demonstrates that the H—H distances remain large enough to allow for an extended structure using either XLT and XGT site models for $Cd(OH)_2$ at least at lower pressure. That the asymmetry parameter increases rapidly to 5 GPa, and becomes much less sensitive to pressure above 10 GPa, may indicate that diverse styles of disordering coexist below 5 GPa.

Another possibility for the cause of the asymmetry of the OH-stretching vibration is changes in the Cd–O sublattice, e.g., distortion in the brucite-type structure. There are some minor changes observed in the lattice modes of $Cd(OH)_2$ below 21 GPa which could support this hypothesis, namely the appearance of weak new modes (ν_3 and ν_6) and a slope change in the pressure-induced shift of the librational mode. Our X-ray diffraction measurements do not resolve any significant changes in the crystal structure below 21 GPa, but it is possible that a modification or distortion of the Cd–O sublattice occurs below 21 GPa and affects the disordering of the H sublattice.

So far no crystalline-to-crystalline phase transition associated with H-sublattice amorphization has been reported for the brucite-type hydroxdies at high pressure. The appearance of many new modes and disappearance of the modes of the low-pressure phase in the lattice-mode range suggest that the Cd–O sublattice undergoes a crystalline-to-crystalline transition. Furthermore, our diffraction measurements show new diffraction lines and a discrete change in relative positions of (010) and (011) lines above 21 GPa, which can be also related to a crystalline-to-crystalline transition.

While the H sublattice undergoes gradual disordering at 5–20 GPa, the disordering seems to be affected by the change in the Cd–O sublattice at 21 GPa: A_{1g}(OH) mode drops by 23 cm^{-1} at 20 GPa just before the amorphization of the H sublattice and a weak yet relatively sharp mode (ν_7) appears at 3588 cm^{-1} after the phase transition. This indicates that the H sublattice may be almost completely disordered near 20 GPa but due to the transition at least part of the H sublattice is reorganized.

This can be supported by our observation during decompression. The high-pressure phase exists metastably below 21 GPa based on the observed lattice modes. In addition, during decompression, ν_7 gains intensity and A_{1g}(OH) mode shift is distinct from that observed during compression, at least to 10 GPa where most of the new features in the lattice-mode

range disappear. Thus, the distinct behavior of the modes in the OH-stretching vibrational range indicates that the high-pressure phase may provide a different environment for the H sublattice.

Although the quality of our X-ray diffraction data does not allow us to investigate the crystal structure of the high-pressure phase, due to strong texturing and peak broadening, our Raman spectra can be interpreted in terms of the $Sr(OH)_2$-type structure that was reported as a transformation product for single crystal of $Ca(OH)_2$ at 6 GPa (Ref. 13) (distinct from the amorphization observed in powder samples[11]). Remarkable similarities were reported between the Raman spectra of the high-pressure phase of single-crystal $Ca(OH)_2$ and $Sr(OH)_2$, and it is notable that the c/a ratio and many of bond lengths in $Cd(OH)_2$ are similar to those in $Ca(OH)_2$ (Table I). The spectra of the high-pressure phases of $Cd(OH)_2$ and $Ca(OH)_2$ are also closely similar: A sharper new peak appears on the high-frequency side of the $A_{1g}(OH)$ mode during the phase transition in $Ca(OH)_2$ which is very similar to the new mode we observed near $A_{1g}(OH)$ in $Cd(OH)_2$ (ν_7 in Fig. 2 and 3). Another new mode is observed on the low-frequency side of $A_{1g}(OH)$ in $Ca(OH)_2$ while $A_{1g}(OH)$ disappears, which could be related to the apparent frequency drop of $A_{1g}(OH)$ in $Cd(OH)_2$ (Fig. 3). New modes appears at the lower-frequency shoulder of $A_{1g}(T)$ and the higher-frequency shoulder of $E_g(T)$, which is very similar to ν_2 and ν_4 in $Cd(OH)_2$ (Fig. 2 and 3). In addition, 2–3 weak modes appear at 200–300 cm^{-1} region in $Ca(OH)_2$, which could be related to a broad new feature observed in $Cd(OH)_2$ (ν_1 in Figs 2a and 6). The librational mode in $Ca(OH)_2$ splits to two modes which could be related to $E_g(R)$ and a new peak, ν_5, in $Cd(OH)_2$ (Fig. 6).

V. CONCLUSION

Based on crystal-structural parameters, $Cd(OH)_2$ is expected to show similar behavior as $Ca(OH)_2$ under pressure, yet because it belongs to the transition-metal group[19], $Cd(OH)_2$ may instead behave similarly to the other transition-metal hydroxides, e.g., $Co(OH)_2$. Below 20 GPa, we have observed a negative mode shift and peak broadening of the OH-stretching modes without any significant changes in X-ray diffraction. We interpret this as indicating disordering of the H sublattice, as observed in $Co(OH)_2$, while the Cd–O sublattice remains in the brucite-type structure. The asymmetry of the OH-stretching mode peak shapes

15

under pressure, which has not been reported for other brucite-type hydroxides, suggests the presence of diverse H sites in $Cd(OH)_2$ below 21 GPa, based on similar observations for H–O in other glasses and minerals with disordered H atoms and the models previously examined for $Co(OH)_2$.

At 21 GPa, we observed significant changes in the lattice modes and X-ray diffraction patterns that indicate a crystalline-to-crystalline transition in $Cd(OH)_2$. From the similarity in Raman spectra between the high-pressure phases of $Cd(OH)_2$ and single-crystal $Ca(OH)_2$, we propose that the high-pressure phase of $Cd(OH)_2$ has the $Sr(OH)_2$-type structure. In the high-pressure phase, the H sublattice is largely amorphized. Yet observation of a weak but sharp mode at higher frequency than $A_{1g}(OH)$ supports the existence of new H sites with less interaction between H and O atoms in this high-pressure phase. The high-pressure phase remain metastably during decompression to 10 GPa along with the low-pressure phase (brucite-type) of $Cd(OH)_2$. To our knowledge, this is the first report of amorphization of the H sublattice associated with a crystalline-to-crystalline transition for the brucite-type hydroxides.

Future studies should investigate the disordered sites for H atoms in $Cd(OH)_2$ some of which could be distinct from those observed in the other brucite-type hydroxides. Furthermore, the crystal structure of the high-pressure phase of $Cd(OH)_2$ remains to be solved.

REFERENCES

* Electronic address: `sangshim@mit.edu`

[1] Q. Williams and R. J. Hemley, Annual Review of Earth and Planetary Sciences **29**, 365 (2001).

[2] T. Nagai, T. Hattori, and T. Yamanaka, American Mineralogist **85**, 760 (2000).

[3] J. B. Parise, K. Leinenweber, D. J. Weidner, K. Tan, and R. B. V. Dreele, American Mineralogist **79**, 193 (1994).

[4] J. B. Parise, B. Theroux, R. Li, J. S. Loveday, W. G. Marshall, and S. Klotz, Physics and Chemistry of Minerals **25**, 130 (1998).

[5] T. Nagai, T. Ito, T. Hattori, and T. Yamanaka, Physics and Chemistry of Minerals **27**, 462 (2000).

[6] M. B. Kruger, Q. Williams, and R. Jeanloz, Journal of Chemical Physics **91**, 5910 (1989).

[7] J. H. Nguyen, M. B. Krugeer, and R. Jeanloz, Physical Review B: Condensed Matter **49**, 3734 (1994).

[8] C. Murli, S. M. Sharma, S. K. Kulshreshtha, and S. K. Sikka, Physica B **307**, 111 (2001).

[9] S. Speziale, R. Jeanloz, A. Milner, M. P. Pasternak, and J. M. Zaug, Phys. Rev. B **71**, 184106 (2005).

[10] C. Meade, R. Jeanloz, and R. J. Hemley, in *High-pressure research: application to Earth and planetary sciences*, edited by Y. Syono and M. H. Manghnani (Terra Scientific Publishing Company, 1992), pp. 485–492.

[11] C. Meade and R. Jeanloz, Geophysical Research Letters **17**, 1157 (1990).

[12] T. S. Duffy, R. J. Hemley, and H.-K. Mao, in[33], pp. 211–220.

[13] S. Ekbundit, K. Leinenweber, J. L. Yarger, J. S. Robinson, and M. V.-V. G. H. Wolf, Journal of Solid State Chemistry **126**, 300 (1996).

[14] J. H. Nguyen, M. B. Kruger, and R. Jeanloz, Physical Review Letters **78**, 1936 (1997).

[15] S. R. Shieh and T. S. Duffy, Physical Review B: Condensed Matter **66**, 134301 (2002).

[16] S. Raugei, P. L. Silvestrelli, and M. Parrinello, Physical Review Letters **83**, 2222 (1999).

[17] H.-K. Mao, J. Xu, and P. M. Bell, Journal of Geophysical Research **91**, 4673 (1986).

[18] T. S. Duffy, C. Meade, Y. Fei, H.-K. Mao, and R. J. Hemley, American Mineralogist **80**, 222 (1995).

[19] H. D. Lutz, H. Möller, and M. Schmidt, Journal of Molecular Structue **328**, 121 (1994).

[20] M. C. Martin and W. R. McKinney, Proceedings of the Materials Research Society **524**, 11 (1998).

[21] S.-H. Shim, T. S. Duffy, and T. Kenichi, Earth and Planetary Science Letters **203**, 729

(2002).

[22] A. P. Hammersley, *Fit2d: An introduction and overview*, ESRF Internal Report, ESRF (1997).

[23] T. J. B. Holland and S. A. T. Redfern, Mineralogical Magazine **61**, 65 (1997).

[24] T. S. Duffy and R. J. Hemley, Reviews of Geophysics **33 supplement**, 5 (1995).

[25] P. F. McMillan and R. L. Memmele, American Mineralogist **71**, 772 (1986).

[26] A. K. Kleppe, A. P. Jephcoat, H. Olijnyk, A. E. Slesinger, S. C. Kohn, and B. J. Wood, Physics and Chemistry of Minerals **28**, 232 (2001).

[27] S. C. Kohn, R. A. Brooker, D. J. Frost, A. E. Slesinger, and B. J. Wood, American Mineralogist **87**, 293 (2002).

[28] N. Garg, S. Karmakar, S. M. Sharma, E. Busseto, and S. K. Sikka, Physica B **349**, 245 (2004).

[29] Y. W. Fei and H.-K. Mao, Journal of Geophysical Research **98**, 11875 (1993).

[30] L. Desgranges, G. Calvarin, and G. Chevrier, Acta Crystallographica **52**, 82 (1996).

[31] L. Desgranges, D. Grebille, G. Calvarin, G. Chevrier, N. Floquet, and J.-C. Niepce, Acta Crystallographica **49**, 812 (1993).

[32] J. B. Parise, J. S. Loveday, R. J. Nelmes, and H. Kagi, Physical Review Letters **83**, 328 (1999).

[33] K. A. Farley, ed., *Volatiles in the Earth and solar system*, vol. 341 of *AIP Conference Proceedings* (American Institute of Physics, 1995).

[34] C. Greaves and M. A. Thomas, Acta Crystallographica **B42**, 51 (1986).

[35] C. Mokenhaupt, T. Zeiske, and H. D. Lutz, Journal of Molecular Structue **443**, 191 (1998).

[36] A. N. Christensen and Y. Dusausoy, Acta Chemica Scandinavic **19**, 609 (1972).

[37] L. Hemmingsen, R. Bauer, M. J. Bjerrum, K. Schwarz, P. Blaha, and P. Anderson, Inorganic Chemistry **38**, 2860 (1999).

[38] T. S. Duffy, J. F. Shu, H.-K. Mao, and R. J. Hemley, Physics and Chemistry of Minerals **22**, 277 (1995).

TABLE I: Selected crystal structure parameters of the brucite-type hydroxides. The classification follows that of Ref. 19.

	Main group		Transition-metal group				
	$Mg(OH)_2$	$Ca(OH)_2$	β-$Ni(OH)_2$	β-$Co(OH)_2$	$Fe(OH)_2$	$Mn(OH)_2$	β-$Cd(OH)_2$
Volume (Å^3)	41.02	54.81	38.87	40.60	42.45	45.24	49.78
c/a	1.518	1.368	1.469	1.461	1.411	1.425	1.347
Interlayer spacing (Å)	2.687	2.616	2.553	2.666	2.578	2.594	2.530
M—O (Å)	2.097	2.369	2.073	2.083	2.139	2.196	2.292
O$\cdots$O (Å)	3.244	3.337	3.126	3.237	3.193	3.226	3.236
O—O (Å)	3.148	3.589	3.126	3.178	3.263	3.322	3.495
O$\cdots$H (Å)[a]	2.517	2.663	2.418	2.525	2.449	2.467	2.543
$\angle$O$\cdots$O—H (°)	46.2	51.1	48.3	46.6	50.3	51.0	52.5
Refs	[30]	[31]	[34][b]	[35][b]	[19][b]	[36]	[37]

[a]Thermal correction is not made

[b]Deuterated samples are used

TABLE II: Bulk modulus (K_0) and its pressure derivative (K_0') of the brucite-type hydroxides.

Material	K_0 (GPa)	K_0'	Reference
$Mg(OH)_2$	54.3 ± 1.5	4.7 ± 0.2	Nonhydrostatic, [29]
	42 ± 2	5.7 ± 0.5	Quasi-hydrostatic, [38]
$Ca(OH)_2$	37.8 ± 1.8	5.2 ± 0.7	[11]
β-$Ni(OH)_2$	88.0	4.7	[28]
β-$Co(OH)_2$	73.3 ± 9.5	4.0 [a]	[14]
$Mn(OH)_2$	41 ± 3	4.7 [a]	[4]
β-$Cd(OH)_2$	37.6 ± 2.2	10.6 ± 0.8	This study [b]

[a]Fixed values
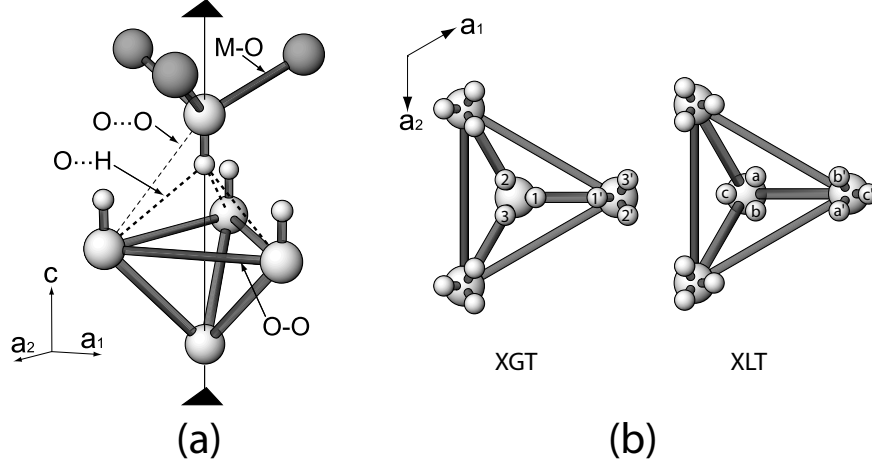
[b]V_0 is fixed to 49.92 Å^3

FIG. 1: The O–H unit and its surroundings in the brucite-type hydroxides. The large dark grey balls, the large light grey balls, and the small balls represent cations, oxygen atoms, and hydrogen atoms, respectively. The notations for various bond lengths used in Table I are shown in **(a)**. **(b)** Projections of the structures along the c-axis for two different H disordering models, i.e., three-site disordered models. In these models H atoms are displaced from the threefold axis and occupy $6i$ $(x, 2x, z)$ sites. XGT represents a case with $x > 1/3$ and XLT represents a case with $x < 1/3$. The individual sites are labeled following the notation used in Ref.[32].
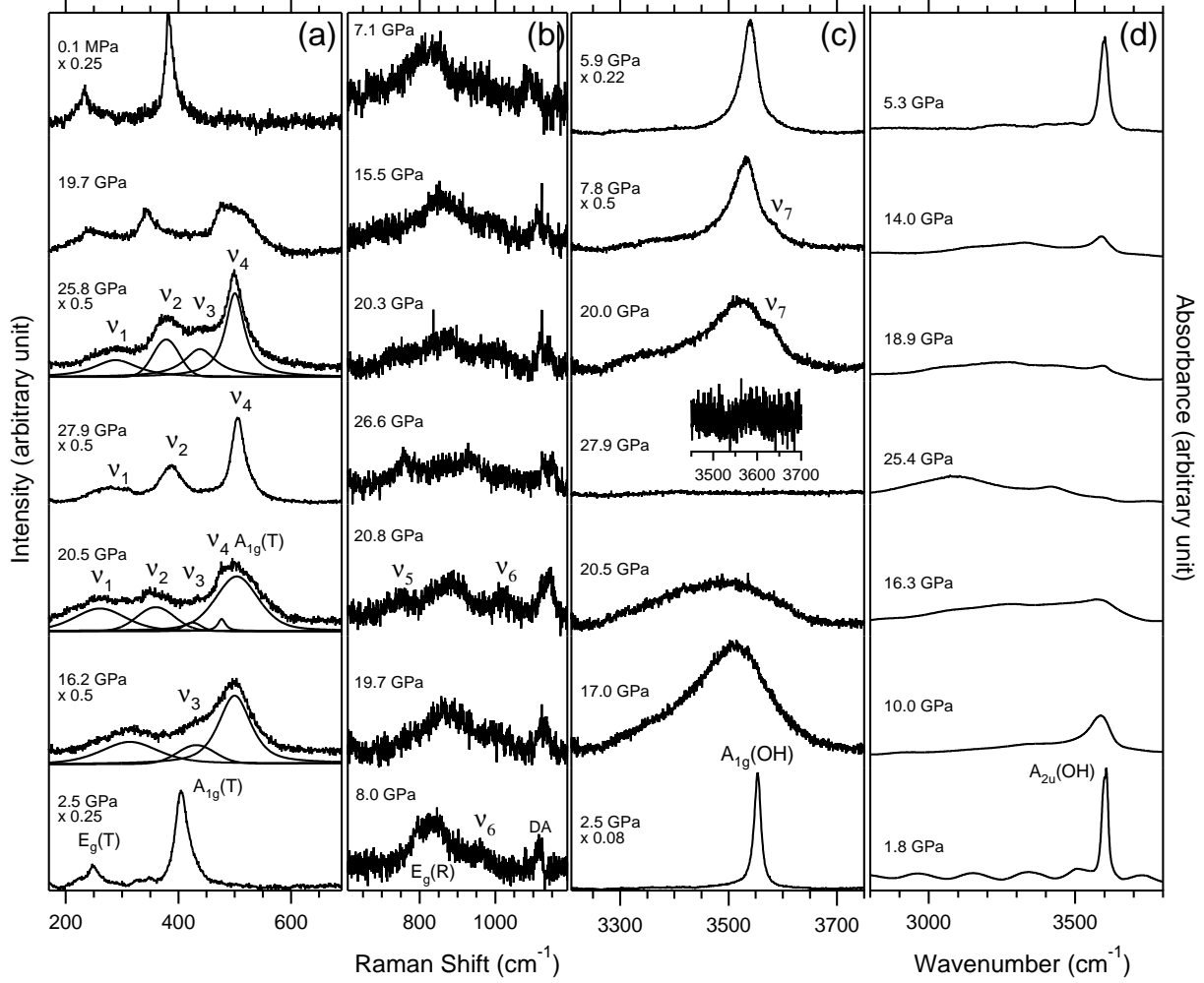
FIG. 2: Vibrational spectra of $Cd(OH)_2$ at high pressure: **(a)** Raman-active lattice modes, $E_g(T)$ and $A_{1g}(T)$, **(b)** Raman-active librational mode, $E_g(R)$, **(c)** Raman-active OH-stretching mode, $A_{1g}(OH)$, and **(d)** IR-active OH-stretching mode, $A_{2u}(OH)$. The backgrounds are subtracted from the spectra. In each sub-figure, the bottom four spectra are measured during compression and the top three spectra are measured during decompression. The spectra shown in (a) are measured during quasi-hydrostatic runs except for the spectra at 16.2 and 25.8 GPa. The spectra shown in (b) are measured during non-hydrostatic runs. The spectra shown in (c) and (d) are measured during quasi-hydrostatic runs. The inset in (c) shows a very weak peak existing at 3588 cm^{-1} observed at 27.9 GPa, ν_7. This becomes more visible during decompression. In (a), some peak fitting results are presented together with measured spectra.
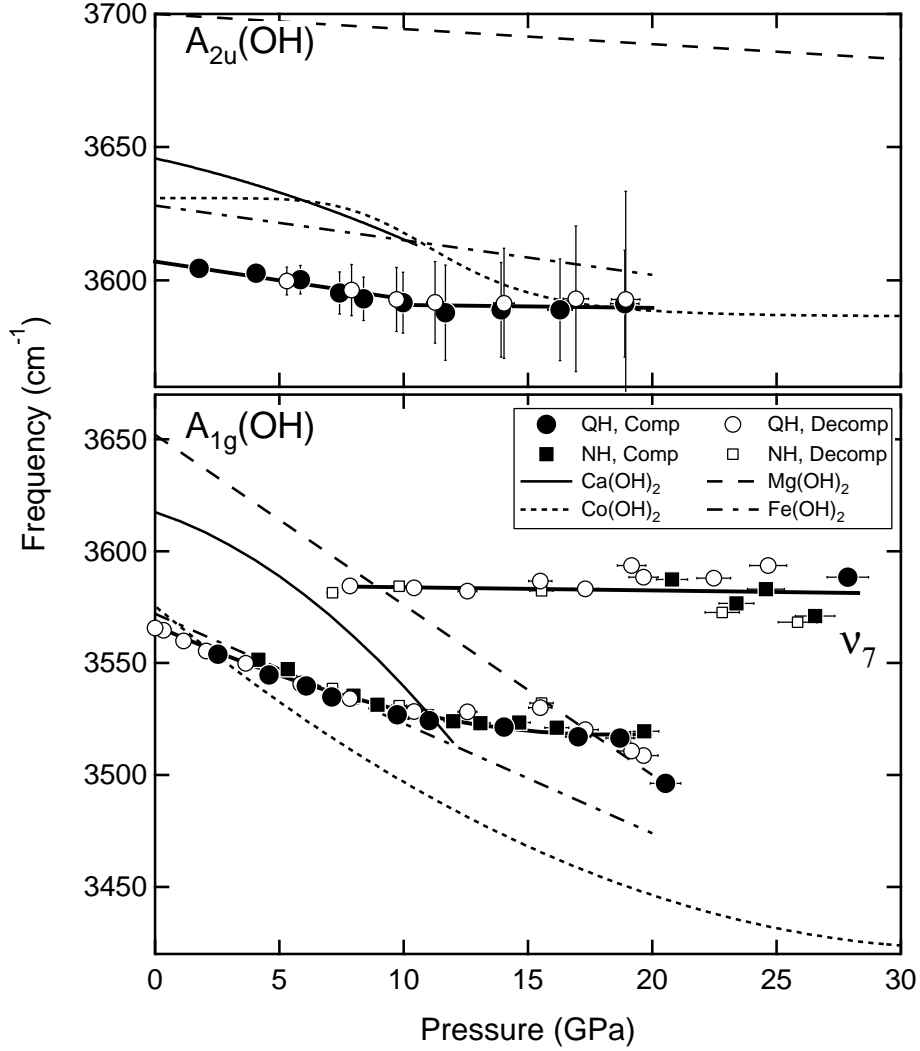
FIG. 3: Pressure-induced shift of the OH-stretching modes of $Cd(OH)_2$. Solid and open symbols represent compression and decompression data, respectively. Circle and square symbols represent runs with and without Ar pressure medium, respectively. The thick solid lines are guides for the eye. The OH-stretching modes of the other hydroxides are shown for comparison: solid lines are for $Ca(OH)_2$ [$A_{2u}(OH)$ from Ref.[6] and $A_{1g}(OH)$ from Ref.[12]], dashed lines are for $Mg(OH)_2$ [$A_{2u}(OH)$ from Ref.[6] and $A_{1g}(OH)$ from Ref.[18]], dotted lines are for $Co(OH)_2$ [$A_{2u}(OH)$ from Ref.[7] and $A_{1g}(OH)$ from Ref.[15]], and dash-dotted lines are for $Fe(OH)_2$ [$A_{2u}(OH)$ and $A_{1g}(OH)$ from Ref.[9]]. The error bars represent 1σ uncertainties. New modes observed at high pressure are assigned as ν_i ($i = 1 \sim 7$) in order of lowest frequency.
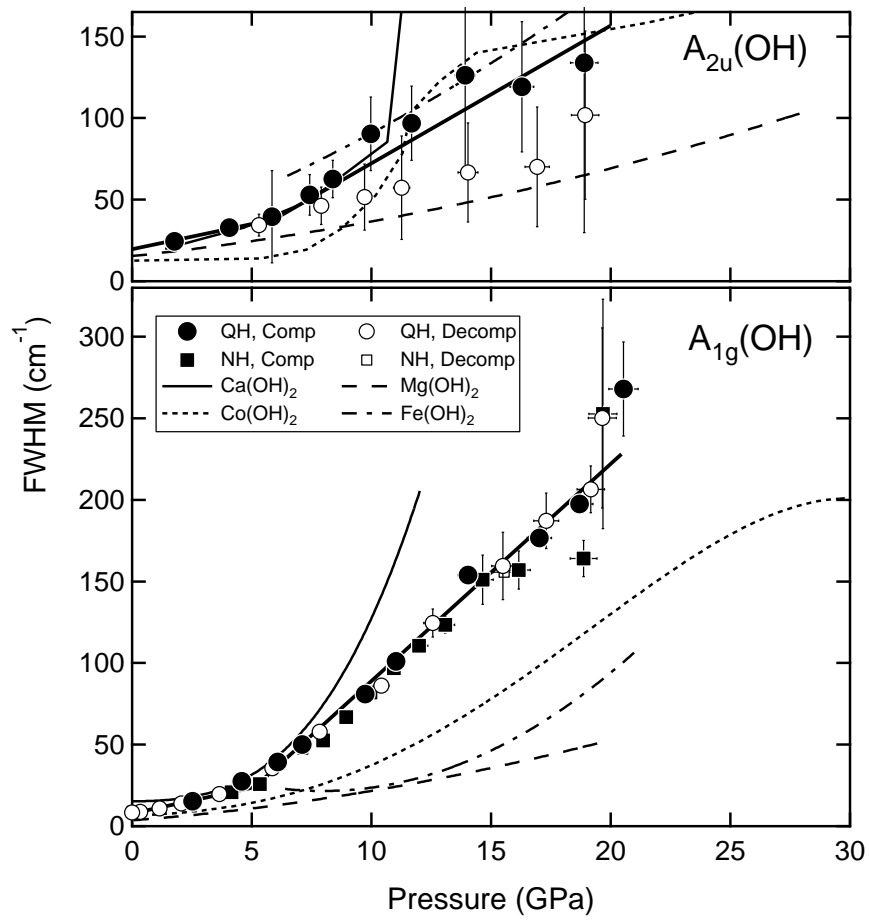
FIG. 4: Full-widths at half maxima (FWHM) of the OH-stretching modes of Cd(OH)$_2$ at high pressure. Notation is the same as in Fig. 3.
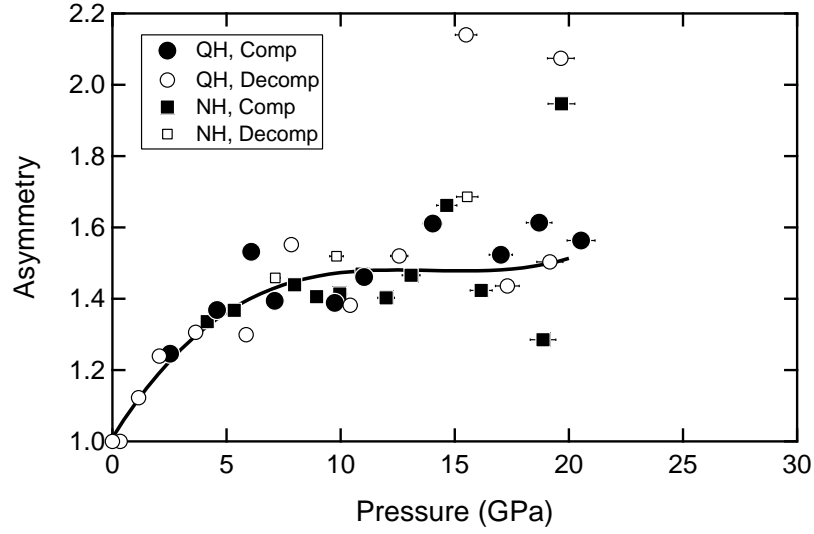
FIG. 5: Asymmetry parameter for the $A_{1g}(OH)$ mode at high pressure. The asymmetry parameter is defined as a ratio of the widths at half maximum between the lower- and higher-frequency sides of a peak fitted by a split pseudo-Voigt function, such that the parameter is 1 for a symmetric peak and 1.5 for a peak that is 50% broader on the lower- side than the higher-frequency side. Notation is the same as in Fig. 3.
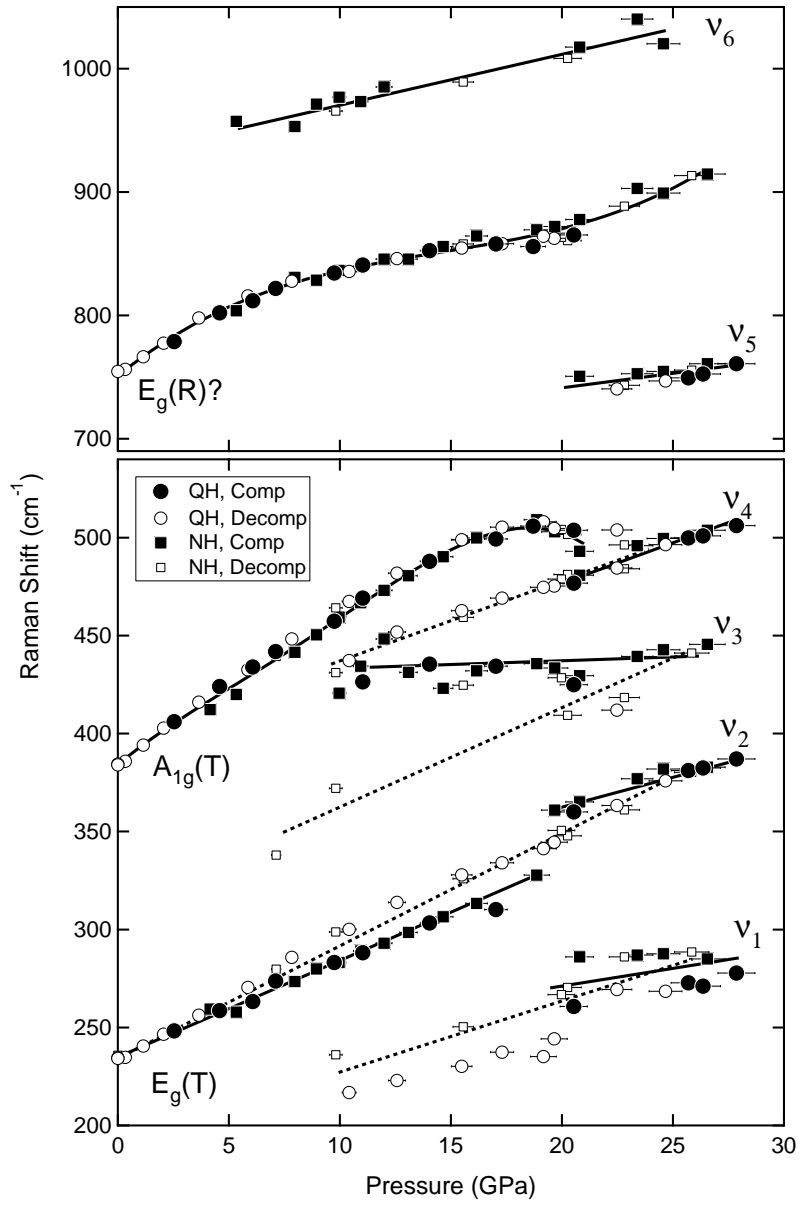
FIG. 6: Pressure-induced shifts of the Raman-active lattice modes and new modes of $Cd(OH)_2$. The solid and dotted lines are guides for the eye for the modes measured during compression and decompression, respectively. Notation is the same as in Fig. 3.
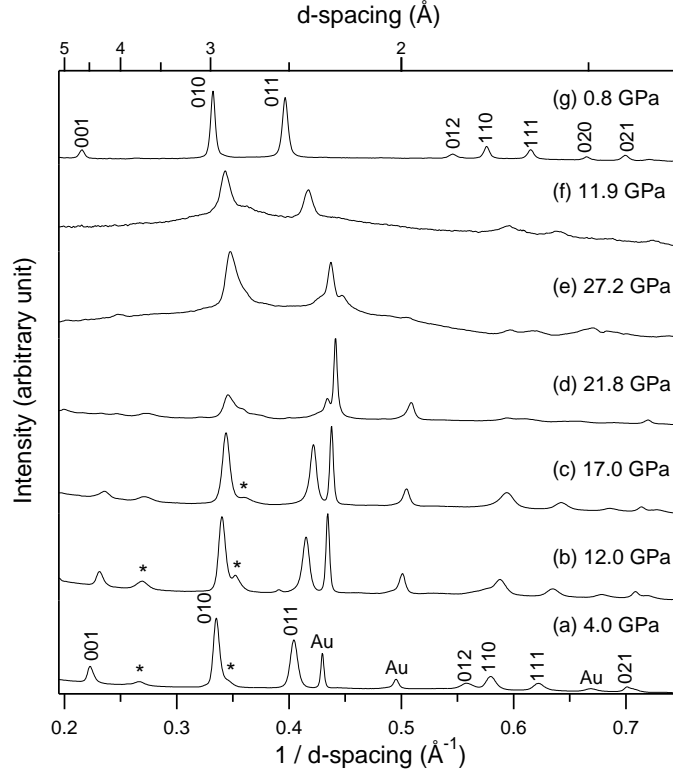
FIG. 7: X-ray diffraction patterns of $Cd(OH)_2$ at high pressures. Patterns (a–d) were measured during compression and (e–g) were measured during decompression. The sample used for pattern (a–d) contains gold pressure calibrant, whereas the sample used for pattern (e–g) does not. Instead, the ruby pressure was used for these patterns. The indexed peaks are from β-$Cd(OH)_2$. The weak peaks at 3.73 and 2.87 Å (marked by asterisk) appeared in some but not all runs at ambient conditions are ascribed to impurities.
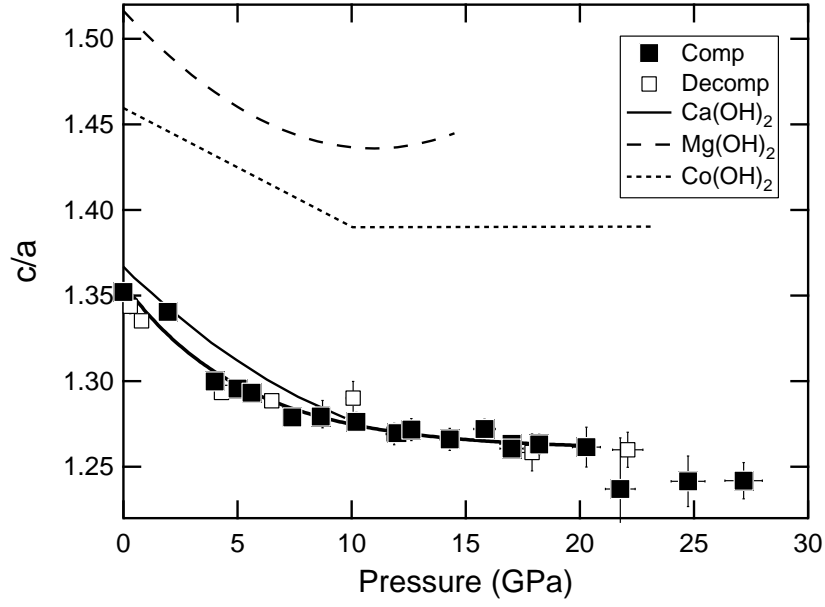
FIG. 8: Pressure-induced changes in the c/a ratio of $Cd(OH)_2$. Sold and open symbols represent compression and decompression data points, respectively. The c/a ratios of the other brucite-type hydroxides are presented for comparison: the solid line is for $Ca(OH)_2$ from Ref.[38], the dashed line is for $Mg(OH)_2$ from Ref.[5], and the dotted line is for $Co(OH)_2$ from Ref.[14].
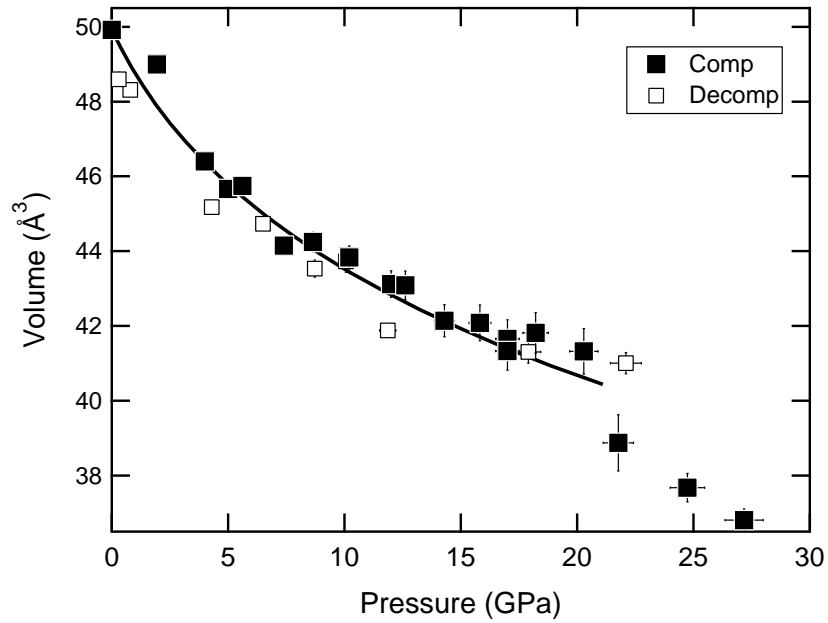
FIG. 9: Volume of $Cd(OH)_2$ measured at high pressures. The solid curve is the fit to the third-order Birch-Murnaghan equation. The last three data points are not included in the fitting. Notation is the same as in Fig. 8.